Identifying the neutrino mass hierarchy with supernova neutrinos

M. Kachelrieß and R. Tomàs
Max-Planck-Institut für Physik (Werner-Heisenberg-Institut), München

Abstract

We review how a high-statistics observation of the neutrino signal from a future galactic core-collapse supernova (SN) may be used to discriminate between different neutrino mixing scenarios. Most SN neutrinos are emitted in the accretion and cooling phase, during which the flavor-dependent differences of the emitted neutrino spectra are small and rather uncertain. Therefore the discrimination between neutrino mixing scenarios using these neutrinos should rely on observables independent of the SN neutrino spectra. We discuss two complementary methods that allow for the positive identification of the mass hierarchy without knowledge of the emitted neutrino fluxes, provided that the 13-mixing angle is large, $\sin^2\vartheta_{13} \gg 10^{-5}$. These two approaches are the observation of modulations in the neutrino spectra by Earth matter effects or by the passage of shock waves through the SN envelope. If the value of the 13-mixing angle is unknown, using additionally the information encoded in the prompt neutronization ν_e burst—a robust feature found in all modern SN simulations—can be sufficient to fix both the neutrino hierarchy and to decide whether ϑ_{13} is "small" or "large."

1 Introduction

Despite the enormous progress of neutrino physics in the last decade, many open questions remain to be solved. Among them are two, the mass hierarchy—normal versus inverted mass spectrum—and the value of the 13-mixing angle ϑ_{13}, where the observation of neutrinos from a core-collapse supernova (SN) could provide important clues [1, 2, 3]. Schematically, the neutrino emission by a SN can be divided into four stages: Infall phase, neutronization burst, accretion, and Kelvin-Helmholtz cooling phase. Most SN neutrinos are emitted during the last two stages, in all flavors with only small differences between the $\bar\nu_e$ and $\bar\nu_{\mu,\tau}$ spectra. Moreover, the absolute values of the average neutrino energies as well as the relative size of the luminosities during the accretion and cooling phases cannot be determined with sufficient precision, especially if the SN is optically obscured and the progenitor type remains unknown. Therefore, a straightforward extraction of oscillation parameters from the bulk of the SN neutrino signal seems hopeless. Only features in the detected neutrino spectra that are independent of unknown SN parameters should be used in such an analysis.

The two most promising sources for such features are the modulations in the neutrino spectra caused by the Earth matter or by the passage of shock waves through the SN envelope. In the first case, matter effects on SN neutrinos traversing the Earth give rise to specific frequencies in the energy spectrum of these neutrinos, which are analytically known and depend only on the neutrino properties and the distance traveled through the Earth [4, 5, 6]. In the other case, the passage of the SN shock waves through the density region corresponding to resonant neutrino oscillations with the atmospheric neutrino mass difference imprints specific time- and energy-dependent modulations on the neutrino energy spectrum [7, 8], difficult to be mimicked by other effects. Only the amplitude of both modulations, and thus the statistical confidence to detect them, depends on how different the emitted neutrino fluxes are, while the specific shape of the modulations is independent from the fluxes.

Case	Hierarchy	$\sin^2\vartheta_{13}$	Earth	Shock	ν_e burst
A	Normal	$\gtrsim 10^{-3}$	Yes	No	No
B	Inverted	$\gtrsim 10^{-3}$	No	Yes	Yes
C	Any	$\lesssim 10^{-5}$	Yes	No	Yes

Table 1: The presence of Earth-matter and shock wave effects in the $\bar{\nu}_e$ spectra and of the ν_e burst for different neutrino mixing scenarios.

In the following sections we will concentrate on three different neutrino mixing schemes (A, B, C), cf. Tab. 1, where modulations by Earth or SN shock effects are clearly separated. For an inverted hierarchy and intermediate values of the 13-mixing angle, $10^{-5} \lesssim \sin^2\vartheta_{13} \lesssim 10^{-3}$, both effects can be present. In this case, the value of ϑ_{13} has to be close to 10^{-5}, the lower limit of the intermediate range. In Fig. 1 we show schematically the sensitivity of several SN observables to different neutrino mixing parameters.

If at the time of the SN detection the value of ϑ_{13} is known to be "large," then the neutrino mass hierarchy can be identified observing the modulations induced either by the SN shock wave propagation (case B in Tab. 1) or by the Earth matter effects (case A). If the value of ϑ_{13} is still unknown and Earth matter effects are observed, an ambiguity exists between case A and C. In sec. 4, we discuss why the neutrino emission during the neutronization burst is only weakly dependent on variations in the input of current SN models and how the neutronization burst can be used to break the degeneracy between A and C.

2 Identifying signatures of the SN shock wave propagation

The neutrino spectra F_{ν_i} arriving at the Earth are determined by the primary neutrino spectra $F^0_{\nu_i}$ as well as the neutrino mixing scenario, $F_{\nu_i}(E,t) = \sum_j p_{ji}(E,t) F^0_{\nu_j}(E,t)$, where

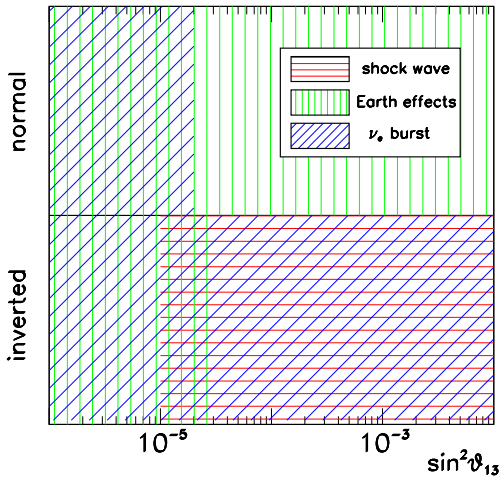

Figure 1: Sensitivity of the three SN observables discussed in the text to different neutrino mixing scenarios.

p_{ji} is the conversion probability of a ν_j into ν_i after propagation through the SN mantle. The probabilities p_{ji} are basically determined by the number of resonances that the neutrinos traverse and their adiabaticity. Both are directly connected to the neutrino mixing scheme. In contrast to the solar case, SN neutrinos must pass through two resonance layers: the H-resonance layer at $\rho_{\rm H} \sim 10^3$ g/cm^3 corresponding to $\Delta m^2_{\rm atm}$, and the L-resonance layer at $\rho_{\rm L} \sim 10$ g/cm^3 corresponding to $\Delta m^2_{\odot}$. Whereas the L-resonance is always adiabatic and in the neutrino channel, the adiabaticity of the H-resonance depends on the value of ϑ_{13}, and the resonance shows up in the neutrino or antineutrino channel for a normal or inverted mass hierarchy respectively [1].

During approximately the first two seconds after core bounce, the neutrino survival probabilities are constant in time and in energy for all three cases A, B, and C. However, at $t \approx 2$ s the H-resonance layer is reached by the outgoing shock wave, see the left panel of Fig. 2. The way the shock wave passage affects the neutrino propagation strongly depends on the neutrino mixing scenario: cases A and C will not show any evidence of shock wave propagation in the observed $\bar{\nu}_e$ spectrum, either because there is no resonance in the antineutrino channel as in scenario A, or because the resonance is always strongly non-adiabatic as in scenario C. However, in scenario B, the sudden change in the density breaks the adiabaticity of the resonance, leading to observable consequences in the $\bar{\nu}_e$ spectrum.

The key ingredient to observe signatures of the shock wave propagation is the time and energy dependence of the neutrino survival probability. In the right panel of Fig. 2, we show $\bar{p}(E,t) \equiv p_{\bar{\nu}_e\bar{\nu}_e}$ averaged with the energy resolution function of Super-Kamiokande, for the case with a forward and a reverse shock. The latter forms when a neutrino-driven baryonic wind develops and collides with the earlier, more slowly expanding SN ejecta. Although the exact propagation history depends on the detailed dynamics during the early stages of

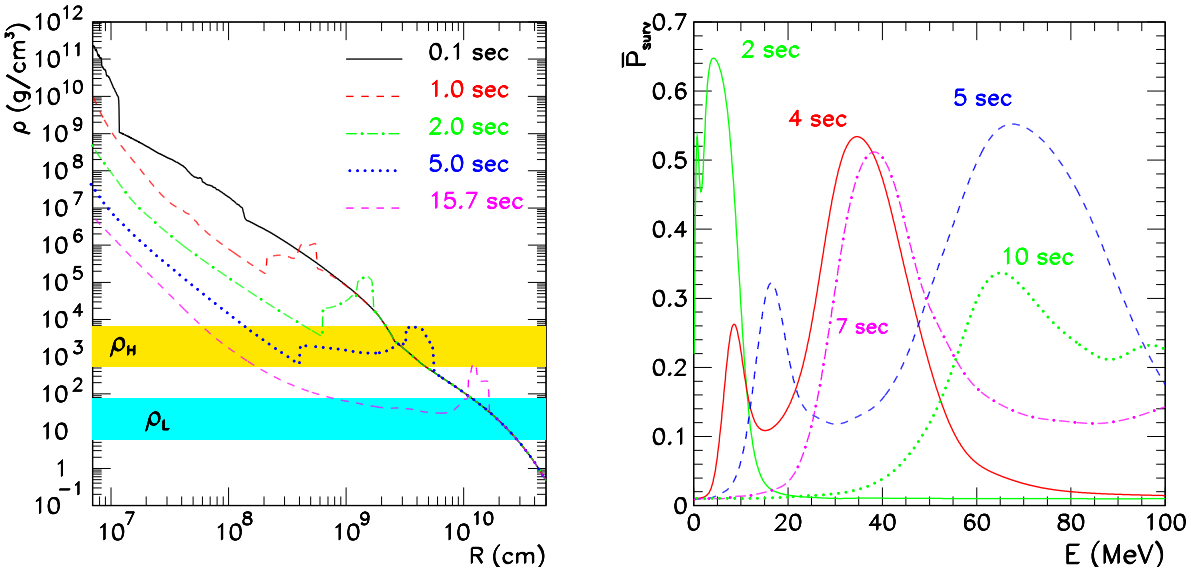

Figure 2: Left: Shock and reverse-shock propagation. The density profile is shown at the indicated instances after core bounce. The density region $\rho_{\rm H}$ corresponds to resonant neutrino oscillations with the atmospheric mass difference, $\rho_{\rm L}$ to the solar one [8]. Right: Survival probability $\bar{p}(E,t)$ as function of energy at different times [8].

the SN explosion, a reverse shock forms in all models which were computed with sufficient resolution [8]. The presence of two shocks results in a dip in $\bar{p}(E,t)$ at those energies for which the resonance region is passed by both shock waves. All these structures move in time towards higher energies, as the shock waves reach regions with lower density.

A useful observable to detect effects of the shock propagation is the average of the measured positron energies, $\langle E_e \rangle$, produced in inverse beta decays $\bar{\nu}_e + p \rightarrow n + e^+$. In Fig. 3, we show $\langle E_e \rangle$ together with the one sigma errors expected for a megaton water Cherenkov detector and a SN in 10 kpc distance, with a time binning of 0.5 s: Both panels contains the case that no shock wave influences the neutrino propagation, the case of only a forward shock wave and of both forward and reverse shock wave. The left and right panels show two different models for neutrino fluxes: G1 assumes different average energies of the emitted neutrinos, $\langle E_0(\nu_x)\rangle/\langle E_0(\bar{\nu}_e)\rangle = 1.2$, and similar fluxes, $\Phi_0(\nu_e)/\Phi_0(\nu_x) = 0.8$, while G2 assumes identical energy spectra, $\langle E_0(\nu_x)\rangle/\langle E_0(\bar{\nu}_e)\rangle = 1$, and $\Phi_0(\nu_e)/\Phi_0(\nu_x) = 0.5$.

The effects of the shock wave propagation are clearly visible, independent of the assumptions about the initial neutrino spectra. Moreover, it is not only possible to detect the shock wave propagation in general, but also to identify the specific imprints of the forward and reverse shock versus the forward shock only case. The signature of the reverse shock is its double-dip structure compared to the one-dip of a forward shock only. To study the dependence of the double-dip structure on the value of ϑ_{13}, we show $\langle E_e \rangle$ as function of time for different 13-mixing angles in the left panel of Fig. 4. Even for as small values as

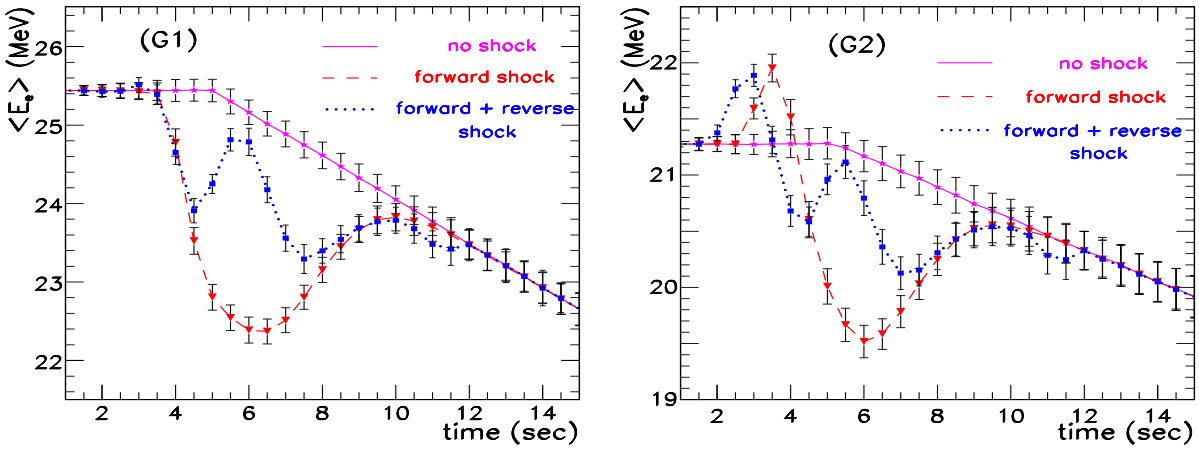

Figure 3: The average energy of $\bar{\nu}p \to ne^+$ events binned in time for a static density profile (magenta), a profile with only a forward shock (red) and with forward and reverse shock (blue). The error bars represent 1 σ errors in any bin, from Ref. [8].

$\tan^2\vartheta_{13} = 5\times10^{-5}$ the double-dip is still clearly visible, while for $\tan^2\vartheta_{13} = 1\times10^{-5}$ only a bump modulates the neutrino signal.

In the right panel of Fig. 4, we show the number of events binned in energy intervals of 10 MeV as function of time for the case of a reverse shock. We can observe clearly how the positions of the two dips change in each energy bin. It is remarkable that the double-dip feature allows one to trace the shock propagation: Given the neutrino mixing scheme, the neutrino energy fixes the resonance density. Therefore, the progress of the shock fronts can be read off from the position of the double-dip in the neutrino spectra of different energy. Thus, the observation of shock wave effects does not only identify case B (inverted hierarchy, large ϑ_{13}), but gives also access to physics deep inside the SN.

3 Earth-matter effects

During the first two seconds after post-bounce, during which roughly half of all neutrinos are emitted, the dependence of the probability to reach the Earth on the neutrino energy E is very weak. However, if neutrinos cross the Earth before reaching the detector, the conversion probabilities may become energy-dependent and induce modulations in the neutrino energy spectrum. These modulations may be observed in the form of local peaks and valleys in the spectrum of the event rate $\sigma F_{\bar{e}}^D$ plotted as a function of $1/E$. These modulations arise in the antineutrino channel only in cases A and C. Therefore its observation would exclude case B. This distortion in the spectra could be measured by comparing the neutrino signal at two or more different detectors such that the neutrinos travel different distances through the Earth before reaching them [4, 9]. However these Earth matter effects can be also identified in a single detector [5, 6].

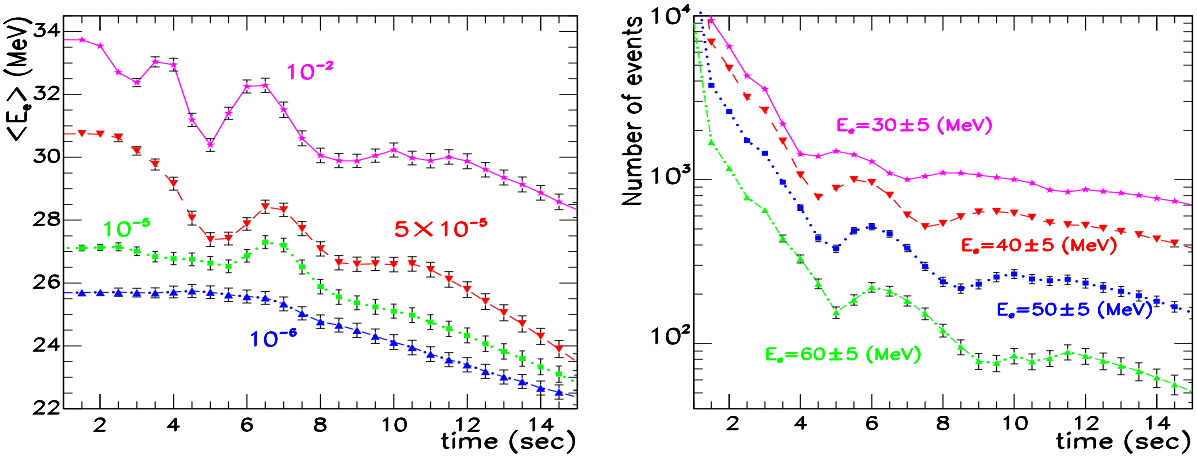

Figure 4: Left: Time dependence of $\langle E_e \rangle$ for a profile with a forward and reverse shock for several values of $\tan^2 \vartheta_{13}$ as indicated. Right: Number of events binned per energy decade as function of time for forward and reverse shock, from Ref. [8].

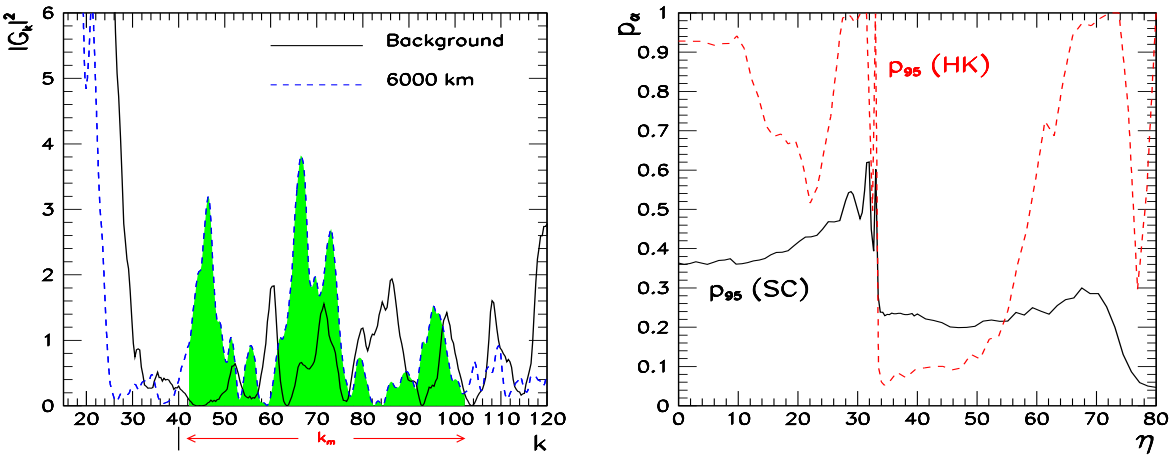

Figure 5: Left: Realistic power spectrum from a single simulation [6]. Right: Comparison of p_{95} as a function of nadir angle η using a "floating cut" as discussed in Ref. [6] for a 32 kton scintillator (SC) and a megaton water Cherenkov (HK) detector.

The net $\bar{\nu}_e$ flux at the detector may be written in the form

$$F_{\bar{e}}^D = \sin^2\vartheta_{12} F_{\bar{x}}^0 + \cos^2\vartheta_{12} F_{\bar{e}}^0 + \Delta F^0 \sum_{i=1}^{7} \bar{A}_i \sin^2(k_i y/2)\,, \tag{1}$$

where y is the "inverse energy" parameter $y \equiv 12.5\ \mathrm{MeV}/E$, $\Delta F^0 \equiv (F_{\bar{e}}^0 - F_{\bar{x}}^0)$ depends only on the primary neutrino spectra, whereas the $\bar{A}_i$ depend only on the mixing parameters and are independent of the primary spectra.

The last term in Eq. (1) is the Earth oscillation term that contains up to seven analytically known frequencies k_i in y, the coefficients $\Delta F^0 \bar{A}_i$ being relatively slowly varying functions of y. The first two terms in Eq. (1) are also slowly varying functions of y, and hence contain frequencies in y that are much smaller than the k_i. The frequencies k_i are completely independent of the primary neutrino spectra, and can be determined to a good accuracy from the knowledge of the solar oscillation parameters, the Earth matter density, and the position of the SN in the sky [6]. The latter can be determined with sufficient precision even if the SN is optically obscured using the pointing capability of water Cherenkov neutrino detectors [10].

The power spectrum of N detected neutrino events is

$$G(k) \equiv \frac{1}{N} \left| \sum_{i=1}^{N} e^{iky_i} \right|^2 . \tag{2}$$

In the absence of Earth effect modulations, $G(k)$ has an average value of one for $k \gtrsim 40$. The region $k \lesssim 40$ is dominated by the "0-peak", cf. Fig. 5, which is a manifestation of the low frequency terms in Eq. (1). Identifying Earth effects is equivalent to observing excess power in $G(k)$ around the known frequencies k_i. The area under the power spectrum between two fixed frequencies $k_{\min}$ and $k_{\max}$ is on an average $(k_{\max} - k_{\min})$. In the absence of Earth effects, this area will have a distribution centered around this mean. The Earth effect peaks tend to increase this area. The confidence level of peak identification, p_α, may then be defined as the fraction of the area of the background distribution that is less than the actual area measured.

In the right panel of Fig. 5, we assume the model G1 for the neutrino fluxes and compare the results obtained with a 32 kton scintillator detector and a megaton water Cherenkov detector. In the latter case, as neutrinos travel more and more distance in the mantle the peak moves to higher k values, and due to the high k suppression, the efficiency of peak identification decreases. When the neutrinos start traversing the core, additional low k peaks are generated and the efficiency increases again.

The identification of Earth matter effects excludes case B, and is thus complementary to the observation of shock wave effects.

4 Neutronization ν_e burst

If the value of ϑ_{13} is unknown, a degeneracy exists between case A and C. Both scenarios predict the same $\bar{\nu}_e$ signature in a water Cherenkov detector, and therefore the previous

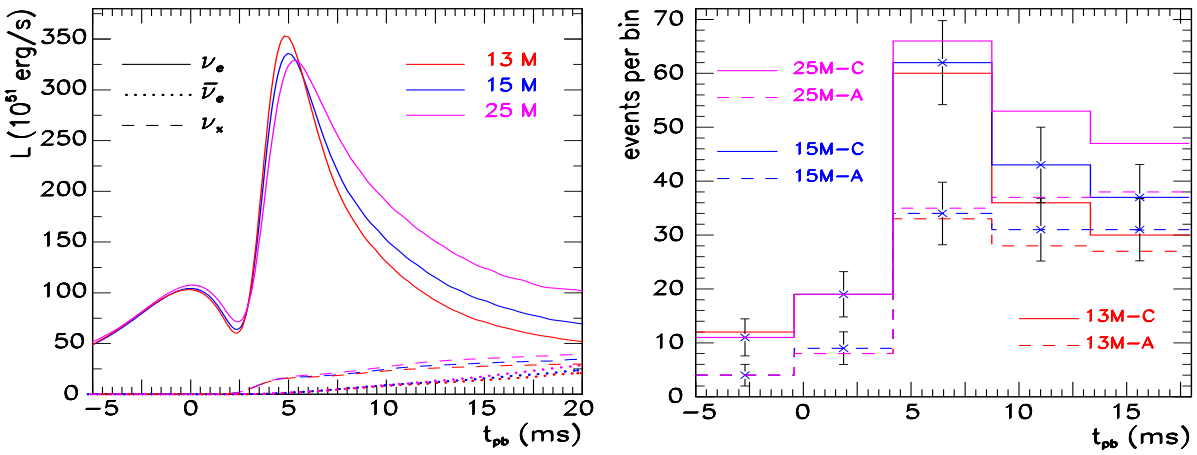

Figure 6: Left: Neutrino luminosities as function of time for different progenitor masses. Right: Number of events per time bin for different reactions in a megaton water Cherenkov detector for a SN at 10 kpc for cases A (dashed lines) and C (solid lines) and for different progenitor masses. Statistical errors are also shown for the 15 $M_\odot$ case. From Ref. [11].

two observables are not useful to disentangle them. In this case, the additional information encoded in the ν_e neutrinos emitted during the neutronization burst can fix the range of ϑ_{13} as well as the neutrino mass hierarchy.

The prompt neutronization burst takes place during the first $\sim$ 25 ms after the core bounce with a typical full width half maximum of 5–7 ms and a peak luminosity of 3.3–$3.5{\times}10^{53}\,\mathrm{erg\,s^{-1}}$. The striking similarity of the neutrino emission characteristics despite the variability in the properties of the pre-collapse cores is caused by a regulation mechanism between electron number fraction and target abundances for electron capture which establishes similar electron fractions in the inner core during collapse. This leads to a convergence of the structure of the central part of the collapsing cores and only small differences in the evolution of different progenitors until shock breakout. The small dependence of the neutronization burst on, e.g., the progenitor mass can be verified in Fig. 6, left panel (cf. also Refs. [11, 12]).

Theoretically, the identification of the neutronization burst is cleanest with a detector using the charged-current absorption of ν_e neutrinos, the most abundant flavor during the burst. Examples of such detectors are heavy water detectors like SNO or liquid argon detectors like ICARUS [13]. The simplest possible observable to identify the neutronization burst is the total number of ν_e events within an arbitrary fixed period t_{max} after the onset of the neutrino signal. However, the probability that the SN is obscured by dust is as high as $\sim$75%. Without an estimate for the SN distance, the total number of events observed cannot be connected to the SN luminosity and is thus not a useful observable. Instead, the time structure of the detected neutrino signal should be used as signature for the neutronization burst [11].

Since the event number in current and proposed charged-current detectors is not high enough to allow for a detailed time analysis, we discuss only the case of a megaton water Cherenkov detector. A draw-back of this choice is that this detector type does not have a clean signature for the ν_e channel. Instead, one has to consider the ν_e elastic scattering on electrons, which is affected by several backgrounds like inverse beta decay or reactions on oxygen. In Ref. [11], it was shown that this background can be substantially reduced by using angular and energy cuts, as well as Gadolinium to tag neutrons from inverse beta decays. The sample of elastic scattering events still contains the irreducible background of scattering on electrons of other neutrino flavors than ν_e, but this contamination does not affect the possibility to disentangle the different neutrino scenarios.

The time evolution of the signal depends strongly on the neutrino mixing scheme. In case A, the ν_e survival probability is close to zero, and therefore the peak structure observed in the initial ν_e luminosity is absent. On the contrary, in case C, 30% of the original ν_e remain as ν_e whereas 70% are converted into ν_x. Since the cross section of ν_e on electrons is much larger than that of ν_x, the signal is dominated by the contribution of ν_e. These ν_e's follow the time evolution of L_{ν_e}, and thus lead to a clear peak in the signal.

In the right panel of Fig. 6 we show the expected neutrino signal from $t = -5$ to 18 ms for different progenitor masses, and for the mixing scenarios A and C. The peak structure can be clearly seen in case C, but not in case A [11]. Including recent improvements of the electron capture rates or uncertainties in the nuclear equation of state has only little effect on the neutronization peak compared to the size of the statistical fluctuations. Therefore the observation of a peak in the first milliseconds of the neutrino signal would rule out the normal mass hierarchy with "large" ϑ_{13} (case A), breaking the degeneracy between scenario A and C observed in the $\bar{\nu}_e$ channel.

After the neutrino mixing scheme has been established, the robustness of the theoretically predicted event number of the neutronization burst makes a measurement of the distance to a SN located at 10 kpc feasible with a precision of about 5%. Since it is likely that a Galactic SN is optically obscured by interstellar dust and no other distance determination can be used, this new method relying only on neutrinos is very promising.

5 Summary

A reliable determination of neutrino parameters using SN neutrinos should be independent from the primary neutrino fluxes produced during the accretion and cooling phase of the SN. Earth-matter effects and the passage of SN shocks through the H-resonance both introduce unique modulations in the neutrino energy spectrum that allow one their identification without knowledge of the primary neutrino spectra. While the observation of Earth-matter effects in the $\bar{\nu}_e$ energy spectrum rules out case B, modulations in the $\bar{\nu}_e$ time spectrum identify case B. If the value of ϑ_{13} would be known to be large, then the neutrino mass hierarchy would be identified. Otherwise, the detection of the neutronization ν_e peak—a robust feature of all modern SN simulations—can break the remaining degeneracy between A and C.

Acknowledgments

We would like to thank our co-authors R. Buras, A. S. Dighe, H.-Th. Janka, A. Marek, G. G. Raffelt, M. Rampp and L. Scheck for many useful discussions and pleasant collaborations, and T. Schwetz for helpful comments about the manuscript. MK acknowledges support by an Emmy-Noether grant of the Deutsche Forschungsgemeinschaft and RT by a Marie-Curie-Fellowship of the European Community.

References

[1] A. S. Dighe and A. Y. Smirnov, Phys. Rev. D **62**, 033007 (2000) [hep-ph/9907423].

[2] C. Lunardini and A. Y. Smirnov, JCAP **0306** (2003) 009 [hep-ph/0302033].

[3] K. Takahashi and K. Sato, Nucl. Phys. A **718** (2003) 455.

[4] C. Lunardini and A. Y. Smirnov, Nucl. Phys. B **616**, 307 (2001) [hep-ph/0106149].

[5] A. S. Dighe, M. T. Keil and G. G. Raffelt, JCAP **0306**, 006 (2003) [hep-ph/0304150].

[6] A. S. Dighe, M. Kachelrieß, G. G. Raffelt and R. Tomàs, JCAP **0401**, 004 (2004) [hep-ph/0311172].

[7] R. C. Schirato and G. M. Fuller, astro-ph/0205390; G. L. Fogli, E. Lisi, D. Montanino and A. Mirizzi, Phys. Rev. D **68**, 033005 (2003) [hep-ph/0304056].

[8] R. Tomàs, M. Kachelrieß, G. Raffelt, A. Dighe, H.-Th. Janka and L. Scheck, JCAP **0409**, 015 (2004) [astro-ph/0407132].

[9] A. S. Dighe, M. T. Keil and G. G. Raffelt, JCAP **0306**, 005 (2003). [hep-ph/0303210].

[10] R. Tomàs, D. Semikoz, G. G. Raffelt, M. Kachelrieß and A. S. Dighe, Phys. Rev. D **68**, 093013 (2003) [hep-ph/0307050].

[11] M. Kachelrieß R. Tomàs, R. Buras, H.-Th. Janka, A. Marek, and M. Rampp, astro-ph/0412082

[12] K. Takahashi, K. Sato, A. Burrows and T. A. Thompson, Phys. Rev. D **68**, 113009 (2003) [hep-ph/0306056].

[13] I. Gil-Botella and A. Rubbia, JCAP **0310**, 009 (2003) [hep-ph/0307244].